Int. J. Heat Mass Transfer. Vol. 36, No. 14, pp. 3477–3485, 1993
Printed in Great Britain

0017-9310/93 $6.00+0.00

Thermophoretic deposition of absorbing, emitting and isotropically scattering particles in laminar tube flow with high particle mass loading

SUNG HO PARK and SANG SOO KIM†

Department of Mechanical Engineering, Korea Advanced Institute of Science and Technology, Yusong, Taejon, 305–701, Korea

(*Received* 5 *August* 1992 *and in final form* 4 *February* 1993)

Abstract—The effects of particle mass fraction and radiation with isotropic scattering have been analyzed on the thermophoretic transport characteristics. A particle trajectory model has been adopted to predict the particle transport. In addition, the P-1 approximation has been used to evaluate radiation heat transfer. Radiative scattering effect due to the suspended particles tends to increase the thermophoretic deposition. In the case of high particle mass fraction, there exists a minimum value of thermophoretic deposition efficiency depending on the optical thickness and conduction–radiation parameter.

1. INTRODUCTION

THERMOPHORESIS is known as a phenomenon in which small particles suspended in a gas migrate from the hot to the cold zones of the gas. This thermophoretic force is a result of greater momentum transfer from the gas molecules on the hot side of the particles compared to the cold side. Practical applications of particle transport in nonisothermal gas flow are the fabrication of optical waveguide (OWG) preforms, semiconductor devices, heat exchangers and thermal precipitators, etc. Especially in high-intensity materials processing applications (e.g. OWG preform deposition from silica-mist laden combustion products) particle mass loadings often exceed 0.3 [1]. Thus, the understanding of high particle mass loading effects on the thermophoretic deposition is important. Furthermore, in OWG and heat exchangers using high temperature combustion exhaust gas, the radiation effect must be considered. A high efficiency of particle deposition on the tube wall is useful for industrial processes such as the high performance of OWG preform fabrication, but not helpful for the traditional aerosol sampling from the high temperature process. The deposition mechanism of suspended particles in a gas stream generally includes Brownian diffusion, thermophoresis, inertial impaction, and electrostatic effects. One or more mechanisms may dominate the deposition phenomenon depending on the flow, external force condition and particle size.

In most of previous numerical studies of thermophoretic transport, the radiation effect was neglected. Goren [2] studied the particle transport by thermophoresis in a laminar-compressible, boundary layer flow over a flat plate. Epstein [3] showed the particle concentration at the wall in the laminar flow is very close to that in turbulent flow from a vertical plate, and laminar flow in the inclined plates by Garg and Jayaraj [4]. Walker *et al.* [5] studied thermophoretic deposition, and Pratsinis and Kim [6] performed a study of simultaneous diffusion, thermophoresis, and coagulation of 0.001 (μm) particles in non-isothermal laminar tube flows. The thermophoretic transport of fly-ash soot, TiO_2 or MgO particles has been reported experimentally [7–11]. Park and Rosner [1, 12] numerically treated the case of high particle mass loaded laminar forced convection systems assuming a relatively simple axisymmetric self-similar flow. In particular, Morse *et al.* [13] have considered absorbing, nonemitting particles with low enclosure temperature when the particle is produced by laser heating in the MCVD process. Most of these previous studies have been performed without the effect of radiation despite the existence of particles. Therefore, the transport processes of the absorbing, emitting, and scattering particles suspended in the non-isothermal gas flow may result in a significant error in the thermophoretic transport without considering the radiation effect for particle phase, as Goren [2] pointed out. When the particle mass fraction is high, the volumetric heat capacity of particles is high compared to that of the gas. Thus it prolongs the thermal developing length. The increase in particle mass fraction will be accompanied by the increase in absorption coefficient (i.e. optical thickness). When the particle emissivity is high, or the mass fraction of particles is high even if the particle emissivity has a moderate value, radiation and scattering due to particles have great effects on this gas–particle flow system. Recently, Yoa *et al.* [14] presented a qualitative analysis on the thermophoretic deposition of highly absorb-

† Author to whom all correspondence should be addressed.

NOMENCLATURE

C	Cunningham correction factor, $1+Kn(1.257+0.4\exp(-1.1/Kn))$
C_L	thermal loading ratio, $\rho_p C_{pp}/\rho_g C_{pg}$
C_H	specific heat ratio, C_{pp}/C_{pg}
C_{pg}	gas specific heat at constant pressure
C_{pp}	particle specific heat at constant pressure
D_B	Brownian diffusion coefficient of particles
D_p	particle diameter
E	cumulative deposition efficiency
E_T	total deposition efficiency
g_i	gravitational acceleration
G_0	dimensionless zeroth-order moment of intensity defined by equation (14)
I_b	blackbody radiation intensity
I_0	zeroth-order moment of intensity
K	thermophoretic coefficient equation (2)
Kn	Knudsen number, $2\lambda/D_p$
k	conductivity
MF	particle mass fraction defined by equation (22)
N	conduction–radiation parameter
n_p	particle number density
Pe	Peclet number, $Re\ Pr$
Pr	Prandtl number
q_p^r	radiative heat flux for particle phase
R	tube radius
Re	Reynolds number, $U_{av}R/\nu$
r	radial coordinate
Sc	Schmidt number, ν/D_B
Stk	Stokes number
t	dimensionless time
T	mixture temperature
u	mixture velocity in axial direction
U_{av}	average gas velocity over the cross section of tube
$\mathbf{v}$	mixture velocity vector defined by equation (12)
$\mathbf{v}_{p0}$	initial particle velocity vector
v	mixture velocity in radial direction
$\mathbf{v}_T$	thermophoretic velocity vector, equation (1)
v_T	thermophoretic velocity of radial direction
V_p	volume of single particle
$\mathbf{x}_p$	particle position vector
$\mathbf{x}_{p0}$	initial particle position vector
x	axial coordinate.

Greek symbols

α	thermal diffusivity
β	extinction coefficient, $\kappa_0+\sigma_0$
ε	surface emissivity
η	dimensionless radial coordinate, r/R
λ	gas molecular mean free path
θ	dimensionless temperature, T/T_{in}
θ_m	dimensionless mixed-mean temperature, equation (23)
κ_0	absorption coefficient
μ	dynamic viscosity of gas
ν	kinematic viscosity of gas
ξ	dimensionless axial coordinate, x/R
ρ_g	gas density
ρ_p	apparent particle density
ρ_{pin}	apparent particle density at tube inlet
ρ_{pm}	material density of single particle
σ	Stefan–Boltzmann constant
σ_0	scattering coefficient
τ_a	aerodynamic response time
τ_c	mean time between particle-to-particle collision
τ_{flow}	characteristic flow time, R/U_{av}
τ_{mom}	momentum relaxation time
τ_0	optical thickness
τ_T	thermal relaxation time, $\rho_{pm}C_{pp}D_p^2/12k_g$
ω_0	normalized single scattering albedo, equation (14).

Subscript

g	gas
in	tube inlet
p	particle
w	wall surface.

ing, emitting, and nonscattering submicron particles in laminar tube flow. Here we have extended this work by considering absorbing, emitting, and isotropically scattering particles in laminar tube flow with high particle mass loading. Radiation with scattering and particle mass fraction effects on the thermophoretic particle transport are investigated in the absence of coagulation. The governing equations for each phase are treated as two-way coupling; that is, the reciprocal interactions of the gas and particle phase are considered in the momentum and energy equations of each phase.

2. ANALYSIS

2.1. *Governing equations*

Gas–particle flow is a two-phase flow where small particles are suspended in a gas stream. A dilute gas–particle flow is defined as a flow in which the particle motion is controlled by local aerodynamic forces. In a dense gas–particle flow, particle motion is governed by particle–particle collisions. In this study, since the volume fraction of the particles is of order 10^{-3} despite a high particle mass fraction of 0.9, we admit the reciprocal interactions between the gas and particle phase but ignore the interactions between the suspended particles in this study. Thus, the present study is treated as a dilute gas–particle flow ($\tau_a/\tau_c < 1$) [15]. Numerical diffusion and instability increases in the Eulerian approach when particle momentum equation becomes first order PDE (in case of neglecting Brownian diffusion). Especially when the Stokes number is small, the stiffness of the interaction source terms in the momentum and energy equations appears. Therefore we adopt Lagrangian approach for the particle momentum equation.

Hot gas with particles enters a cold tube as a fully developed, incompressible laminar flow. Suspended particles in a hot gas stream are transported in the direction of decreasing temperature and deposit on the tube wall by thermophoresis. The particle deposition on the tube wall is determined from the coupled gas momentum, mixture energy, radiative transport, and particle momentum equation. The thermophoretic velocity, $\mathbf{v}_T$ of a particle in a gas subject to a temperature gradient has been derived by theoretical analysis:

$$\mathbf{v}_T = -K\frac{\nu}{T}\nabla T. \tag{1}$$

This thermophoretic velocity depends on the gas kinematic viscosity (ν), thermophoretic coefficient (K), temperature, and temperature gradient. Thermophoretic coefficient depends mainly on the Knudsen number (Kn) and the ratio of the thermal conductivity of the gas to that of the particle. The following formula proposed by Talbot *et al.* [16] was used,

$$K = 2C_s \times \frac{(k_g/k_p + C_t Kn)(1 + Kn(1.2 + 0.41\exp(-0.88/Kn)))}{(1+3C_m Kn)(1+2k_g/k_p + 2C_t Kn)}$$

$$Kn = 2\lambda/D_p. \tag{2}$$

Here, C_s, C_m and C_t are coefficients related to the gas–particle interactions and are equal to 1.149, 1.23 and 2.16, respectively [16].

The following major simplifying assumptions are made in the present investigation.

(1) Flow is a dilute gas–particle flow owing to the low particle volume fraction.

(2) Flows for both particle and gas phase have laminar fully developed velocity profiles at the tube inlet. Temperature distributions of gas and particle phase are uniform at the tube inlet.

(3) Gas and particle properties are independent of the temperature.

(4) Brownian diffusion and coagulation are neglected. The particle Reynolds number is so small that non-Stokes' drag is neglected.

(5) Natural convection is negligible [17].

(6) Particles are spheres of uniform size and their Biot number is small enough to neglect radial variation of temperature within the sphere.

(7) Particles are gray absorbing, emitting, and isotropically scattering, while the gas is transparent to radiation. Absorption coefficient is constant in thermal field.

(8) Photophoretic transport is neglected.

Brownian diffusion is usually negligible in the case that the Brownian diffusivity of particles is very small relative to the gas diffusivity ($Sc \gg 1$). For example, for particles with a size of 0.1 μm at 1000 K, the Brownian diffusion coefficient is of the order of 10^{-9} $m^2\ s^{-1}$. Particle coagulation associated with Brownian motion leads to a reduction in the total number density and increases in the average size, and it is a function of particle number density, particle size and process residence time. Brownian coagulation is neglected because the coagulation characteristic time is much longer than the process residence time when the particle mass fraction is less than 0.5 in this study [1, 6, 18]. With these assumptions the dimensionless governing equations of each phase are as follows:

Gas phase governing equations

$$\frac{\partial}{\partial\xi}(\rho_g u_g) + \frac{1}{\eta}\frac{\partial}{\partial\eta}(\rho_g \eta v_g) = 0 \tag{3}$$

$$u_g\frac{\partial u_g}{\partial\xi} + v_g\frac{\partial u_g}{\partial\eta} = -\frac{\partial p}{\partial\xi} + \frac{1}{Re}\left(\frac{\partial^2 u_g}{\partial\xi^2} + \frac{1}{\eta}\frac{\partial}{\partial\eta}\left(\eta\frac{\partial u_g}{\partial\eta}\right)\right) + \frac{\rho_p}{\rho_g}\frac{u_p-u_g}{Stk} + \frac{\rho_p}{\rho_g}\frac{K}{Stk\,Re}\frac{1}{\theta}\frac{\partial\theta}{\partial\xi} \tag{4}$$

$$u_g\frac{\partial v_g}{\partial\xi} + v_g\frac{\partial v_g}{\partial\eta} = -\frac{\partial p}{\partial\eta} + \frac{1}{Re}\left(\frac{\partial^2 v_g}{\partial\xi^2} + \frac{1}{\eta}\frac{\partial}{\partial\eta}\left(\eta\frac{\partial v_g}{\partial\eta}\right)\right) + \frac{\rho_p}{\rho_g}\frac{v_p-v_g}{Stk} + \frac{\rho_p}{\rho_g}\frac{K}{Stk\,Re}\frac{1}{\theta}\frac{\partial\theta}{\partial\eta}. \tag{5}$$

Particle phase momentum equation

$$\frac{d\mathbf{v}_p(t)}{dt} = \frac{(\mathbf{v}_g-\mathbf{v}_p)}{Stk} - \frac{K}{Stk\,Re}\nabla\ln\theta + \frac{R}{U_{av}^2}g_i \tag{6}$$

$$\mathbf{v}_p(t) = \mathbf{v}_{p0}\exp(-t/Stk) + \left(\mathbf{v}_g - \frac{K}{Re}\nabla\ln\theta + Stk\frac{R}{U_{av}^2}g_i\right)(1-\exp(-t/Stk)) \tag{7}$$

$$\mathbf{x}_p(t) = \mathbf{x}_{p0} + Stk\,\mathbf{v}_{p0}(1-\exp(-t/Stk)) + \left(\mathbf{v}_g - \frac{K}{Re}\nabla\ln\theta + Stk\frac{R}{U_{av}^2}g_i\right) \times (t - Stk(1-\exp(-t/Stk))) \tag{8}$$

where

$$\xi = x/R, \quad \eta = r/R$$

$$Re = \frac{U_{av}R}{\nu} \quad \text{and} \quad Stk = \frac{\rho_{pm}CU_{av}D_p^2}{18\mu R}. \tag{9}$$

The velocity discontinuity (slip) at the surface of a small particle has been modified with the Cunningham correction factor C [18]. An important dimensionless parameter in gas–particle flows is the Stokes number, which represents the ratio of the particle relaxation time τ_{mom} to the flow characteristic time τ_{flow}. If the Stokes number is very small, particles have enough time to respond to the aerodynamic changes in the host gas. In the gas phase momentum equation, the third term of the right hand side represents the momentum exchange (interacting force) between the gas and particles, and the fourth term is attributed to the momentum exchange due to the thermophoretic migration of particles. These two terms can be neglected in the case of low particle mass loading (i.e. $\rho_p/\rho_g \ll 1$). In the particle momentum equation, the right hand side terms represent the drag force of gas on the particle (interacting force), thermophoretic force and particle gravity effect, respectively. The buoyancy effect due to the difference of gas and particle density is generally negligible because $\rho_{pm}(= 1350\ \mathrm{kg\ m^{-3}})$ is much greater than $\rho_g(\rho_{pm}/\rho_g > 1000)$. If the external forces are approximately constant over a small time interval t, particle momentum equation can be integrated twice analytically to obtain the particle velocity $\mathbf{v}_p(t)$ and particle position $\mathbf{x}_p(t)$ during the time interval.

With the neglect of viscous dissipation and expansion work, gas phase energy balance equation is written as:

$$\rho_g C_{pg} v_g \cdot \nabla T_g = \nabla \cdot k_g \nabla T_g + \rho_p C_{pp} \frac{T_p - T_g}{\tau_T} \quad (10)$$

and for particulate phase

$$\rho_p C_{pp} \mathbf{v}_p \cdot \nabla T_p = -\rho_p C_{pp} \frac{T_p - T_g}{\tau_T} - \nabla \cdot q_p^r. \quad (11)$$

Here, the particle temperature is almost the same as the gas temperature because the thermal relaxation time τ_T is very small compared to the characteristic flow time τ_{flow}. To simplify the above phase energy equations, we introduce the mixture variables such as mixture density, mixture velocity and mixture temperature [1, 14, 15, 19]:

$$\begin{aligned} T_p &\cong T_g = T, (\tau_T \ll \tau_{flow}) \\ \rho &\equiv \rho_p + \rho_g \\ \rho C_p T &= \rho_p C_{pp} T_p + \rho_g C_{pg} T_g \\ \rho \mathbf{v} &= \rho_p \mathbf{v}_p + \rho_g \mathbf{v}_g. \end{aligned} \quad (12)$$

The simplified mixture energy equation can be obtained by adding the energy equations of gas and particle phase:

$$\rho_g C_{pg}(1 + C_L)\mathbf{v} \cdot \nabla T = \nabla \cdot k_g \nabla T - \nabla \cdot q_p^r. \quad (13)$$

This mixture energy equation is nondimensionalized by introducing the following quantities.

$$\begin{aligned} &\theta = \frac{T}{T_{in}} \cong \frac{T_g}{T_{in}} \cong \frac{T_p}{T_{in}} \\ &\nabla \cdot q_p^r = \kappa_0(4\pi I_b - I_0) \\ &\kappa_0 = \frac{\pi}{4} D_p^2 n_p \varepsilon_p; \quad \omega_0 = \frac{\sigma_0}{\beta}; \quad \beta = \kappa_0 + \sigma_0 \\ &\tau_0 = \beta R = \frac{\kappa_0}{1-\omega_0} R; \quad N = \frac{k_g \beta}{4\sigma T_{in}^3} \\ &G_0 = \frac{I_0}{4\sigma T_{in}^4}; \quad C_L = \frac{\rho_p C_{pp}}{\rho_g C_{pg}} = \frac{\rho_p}{\rho_g} C_H \\ &Pe = Re\, Pr. \end{aligned} \quad (14)$$

This leads to

$$(1 + C_L)\left(u\frac{\partial \theta}{\partial \xi} + v\frac{\partial \theta}{\partial \eta}\right) = \frac{1}{Pe}\left(\frac{\partial^2 \theta}{\partial \xi^2} + \frac{1}{\eta}\frac{\partial}{\partial \eta}\left(\eta\frac{\partial \theta}{\partial \eta}\right)\right) - \frac{(1-\omega_0)\tau_0^2}{Pe\, N}(\theta^4 - G_0). \quad (15)$$

Boundary conditions:

$$\begin{aligned} &\xi = 0; \quad u_g = 2(1-\eta^2), v_g = 0, \theta = 1 \\ &\xi = 50; \quad \frac{\partial u_g}{\partial \xi} = \frac{\partial v_g}{\partial \xi} = 0, \frac{\partial^2 \theta}{\partial \xi^2} = 0 \\ &\eta = 0; \quad \frac{\partial u_g}{\partial \eta} = 0, v_g = 0, \frac{\partial \theta}{\partial \eta} = 0 \\ &\eta = 1; \quad u_g = v_g = 0, \theta = \theta_w. \end{aligned} \quad (16)$$

Assuming that the dispersed phase is a continuum for the thermal radiation, the absorption coefficient κ_0 has been used in the definition proposed by Echigo *et al.* [20–22]. In the present study, the emissivity of tube wall and particle is taken as 0.7 and 0.9, respectively. Dimensionless variable N represents the gas conduction–particle radiation parameter because we consider only radiation due to particles. The last term in the right hand side of equation (15) represents the contribution of particle radiation that has been modeled with the P-1 approximation [23]. Previous studies indicate that the P-1 approximation is more accurate in the optically thick rather than the optically thin limit. In our study, the optical thickness is 1.612 in the lowest particle mass fraction case of 0.1. The radiative transfer equation in terms of the P-1 approximation and Marshak's boundary conditions are described in a dimensionless form by [23, 24]

$$\left[\frac{\partial}{\partial \xi^2} + \frac{1}{\eta}\frac{\partial}{\partial \eta}\left(\eta\frac{\partial}{\partial \eta}\right)\right] I_0 = 3(1-\omega_0)\tau_0^2(I_0 - 4\pi I_0). \quad (17)$$

Boundary conditions:

$$I_0 \pm \tfrac{2}{3}(1+2\lambda_w)\left(\frac{\partial I_0}{\partial z}\right)_w = 4\pi I_{bw},$$

$$\lambda_w = \frac{1-\varepsilon_w}{\varepsilon_w} \quad \text{and } z = \xi, \eta \quad (18)$$

$$\left(\frac{\partial I_0}{\partial \eta}\right)_{\eta=0} = 0. \tag{19}$$

It can be assumed that the inlet opening section is attached to a reservoir of known temperature, T_{in}. This opening section is nonreflecting and its temperature is the same as that of the reservoir. The temperature of the outlet opening section is unknown but thermally fully developed. Thus the temperature of the next zone near the outlet is almost the same as that of outlet section. The opening of the inlet and outlet tubes are nonreflecting, therefore, the assumption of a pseudo black wall is applied for the radiation boundary conditions in equation (18). At the tube center, the symmetric condition of temperature suggests that zeroth moment intensity I_0 will not change, as given in equation (19).

2.2. *Numerical procedure*

Nonuniform grids have been used in both axial and radial directions. The test of grid size dependence turned out to be less than 1% for (31 × 51) and (51 × 71) grids, thus the grid size (31 × 51) is used throughout this study. The SIMPLER algorithm and power law differencing scheme have been applied for solving the governing equations of gas phase. The momentum equation of particulate phase has been integrated analytically to obtain the velocities and trajectories of particles. A particle is considered to be deposited if it comes within a distance of $D_p/2$ to the tube wall. Cumulative deposition efficiency is defined as the percentage of particles that are deposited on the wall within an axial distance ξ. Equations (4)–(6), (15) and (17) are coupled with one another and iteratively solved up to the maximum error of a 10^{-4} bound.

A total of 1500 starting locations for particles have been uniformly distributed at the tube inlet and each location is assumed to carry a fraction of the total particle mass. The apparent density of dispersed particles ρ_p is defined as $\rho_p = \rho_{pm} n_p V_p$, and is evaluated by particle source-in-cell (PSI-CELL) model [25],

$$\dot{m}_j = X_j \dot{M}_p \tag{20}$$

where X_j is the mass fraction of the particle entering at station j. $\dot{m}_j$ will be constant along the entire trajectory starting at station j. The local apparent density of particle phase in each cell is determined from

$$\rho_p = \sum \dot{m}_j \Delta\tau / V_{cell} \tag{21}$$

where $\Delta\tau$ is the particle residence time in cell and V_{cell} is the cell volume.

The inlet mass fraction of the particles is defined as the ratio of the particle mass flow rate to that of the mixture flow rate.

$$MF = \frac{\dot{M}_p}{\dot{M}_g + \dot{M}_p} = \frac{\rho_{pin}}{\rho_g + \rho_{pin}}. \tag{22}$$

The mixed-mean temperature is the physical quantity of interest in heat transfer study and defined by

$$\theta_m(\xi) = \frac{\int_0^1 \theta(\xi, \eta) u(\eta) \eta \, d\eta}{\int_0^1 u(\eta) \eta \, d\eta}. \tag{23}$$

3. RESULTS AND DISCUSSIONS

The thermophoretic deposition of absorbing, emitting and isotropically scattering particles has been investigated with various dimensionless parameters in laminar tube flow. In order to establish the validity of the present numerical method, two limiting cases were compared in Figs. 1 and 2. P-1 approximation solutions for the coupled energy equation without particle phase agree closely with Pearce and Emery's results [26] shown in Fig. 1. This figure illustrates that the present numerical method for the P-1 approximation can accurately predict the combined heat transfer behaviors. Figure 2 compares, in the absence of radiation, the cumulative deposition efficiency predicted by the present trajectory with that of Walker *et al.* [5]. This verification shows almost negligible difference between these particle transport predictions.

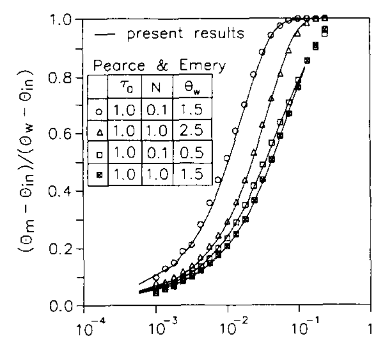

FIG. 1. Mixed-mean temperatures along axial distance with a parabolic velocity distribution.

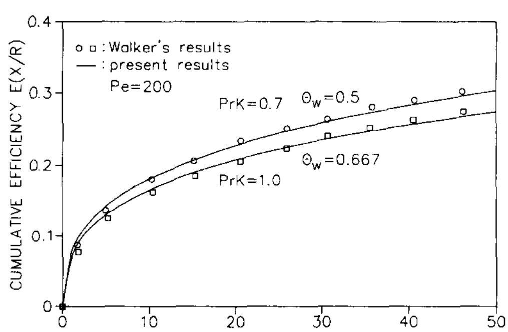

FIG. 2. Cumulative deposition efficiency along axial distance for different conditions.

Figures 3–5 demonstrate the influence of the conduction–radiation parameter N on particle trajectories and thermophoretic particle transport characteristics. By the definition of N in equation (14), the decrease of N means the increase of inlet temperature with fixed particle diameter, mass fraction and scattering albedo ω_0. For smaller N, which means a strong radiation, more rapid thermal development is made. That is, the mixture temperature drops rapidly. Figure 3 shows the effect of N on thermophoretic velocity along radial and axial distances. The thermophoretic velocity v_T close to the tube center approaches zero because of the symmetric condition of the temperature. The thermophoretic velocity decreases with increasing the radiation except for the central core of entrance region ($r/R < 0.4$, $x/R = 10$). With fixed value of N, the thermophoretic velocity increases near the wall. The thermophoretic velocity in the central core of the entrance region increases as the conduction–radiation parameter is reduced to a certain value ($N = 0.1$) and decreases beyond that level of radiation. This behavior is explained by the following reasons. The radiation effect will change the temperature profile from the flat to the curve, which means there exists temperature gradient. Therefore the thermophoretic velocity increases with decreasing N. However, the radiation becomes stronger ($N < 0.1$), the temperature of central core region fully develops, that is, the temperature profile of this region is lower and flattened, thus the thermophoretic velocity decreases. The thermophoretic velocity of particles decreases as particles move downstream, and this phenomenon makes the cumulative deposition efficiency rapidly approach an asymptotic limit. This limit is referred to as the total deposition efficiency, E_T, because this is the value that would be measured far downstream ($x/R = 50$). In addition, in the case of strong radiation, there is no thermophoretic transport in the central core region since the temperature profile becomes flat except in the conduction region near the wall. Cumulative deposition efficiency more quickly reaches some constant value with decreasing N. The thermophoretic velocity and particle trajectories represent a considerable difference according to the value of N (Figs. 3 and 4) and, therefore, the cumulative deposition efficiency E is greatly affected by N (Fig. 5).

Figures 6–8 show the scattering effect of particles on the thermal development and thermophoretic particle transport characteristics. The neglect of the scattering

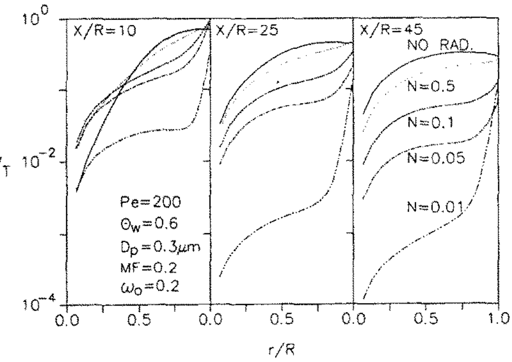

FIG. 3. Effect of conduction–radiation parameter on thermophoretic velocity along radial and axial distance.

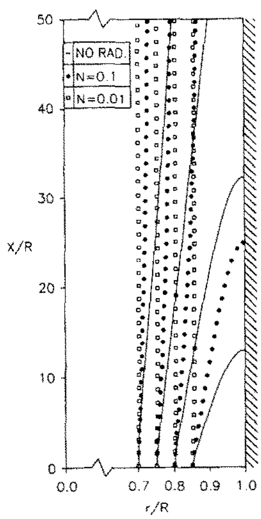

FIG. 4. Effect of conduction–radiation parameter on particle trajectories.

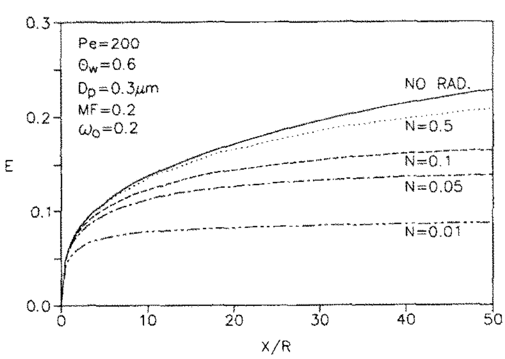

FIG. 5. Cumulative deposition efficiency for various conduction–radiation parameters.

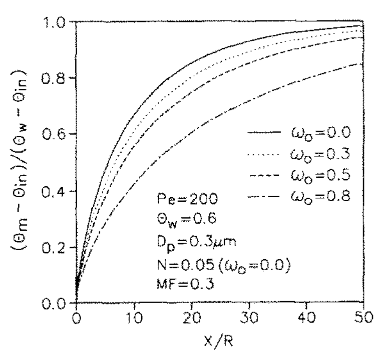

FIG. 6. Effect of scattering albedo on mixed-mean temperature development.

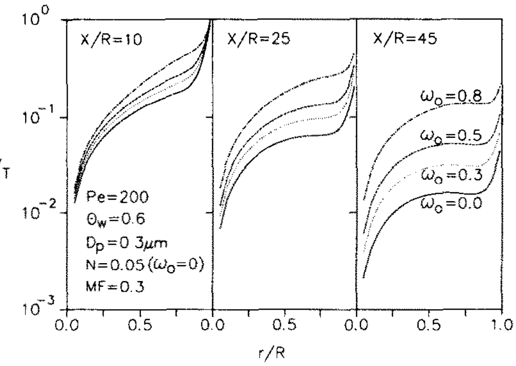

FIG. 7. Effect of scattering albedo on thermophoretic velocity along radial and axial distance.

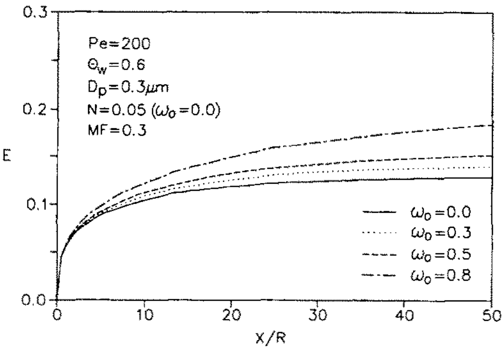

FIG. 8. Cumulative deposition efficiency for various scattering albedo.

in the medium may overpredict the radiative heat transfer [23]. Scattering albedo depends on wavelength, particle diameter and complex index of refraction [27]. Thermal radiation has various wavelengths. Fortunately, the effect of anisotropic scattering is not critical besides very large values of the scattering albedo [19, 23]. Thus, we assume the scattering is isotropic. Here the variation of the scattering albedo can be achieved by using another kind of particle (i.e. different complex index of refraction). The scattering albedo ω_0 represents the fraction of attenuated energy that is the result of scattering. The conduction–radiation parameter N changes with the value of extinction coefficient, and we choose the reference value of $N = 0.05$ based on absorption only (in the case of no scattering). As the scattering albedo ω_0 increases, a higher fraction of the radiation emitted in a high temperature region is scattered near the region of emission rather than traveling and absorbing at the low temperature region. Thus an increase of the scattering albedo decreases the development of mixed-mean temperature even if absorption (i.e. particle mass fraction) is held constant (Fig. 6). The slow development of the mixed-mean temperature makes the steep temperature gradient in the medium and increases the thermophoretic velocity, thus increases the cumulative particle deposition efficiency (Figs. 7 and 8).

Figures 9–11 show the influence of particle mass fraction on the thermal development and the thermophoretic particle transport characteristics. There is very small difference in relative velocities between the particle and the gas because of negligible inertia (small Stokes number, $O(10^{-4})$), thus the effect of particles has been less than 5% on the fully developed gas velocity profile even if the particle mass fraction is high ($MF = 0.7$). An increase in particle mass fraction

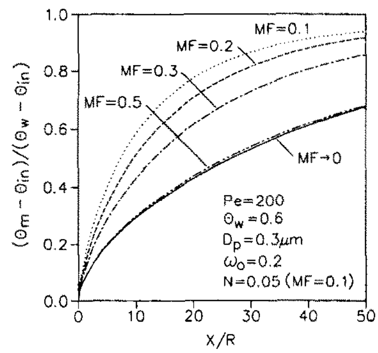

FIG. 9. Effect of particle mass fraction on mixed-mean temperature development.

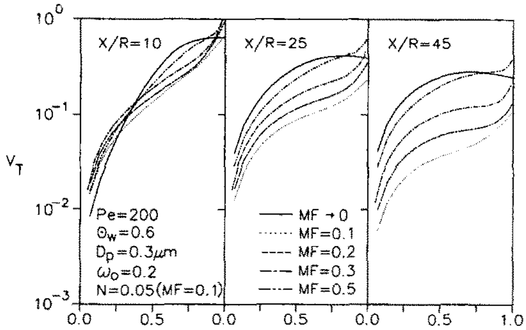

FIG. 10. Effect of particle mass fraction on thermophoretic velocity along radial and axial distance.

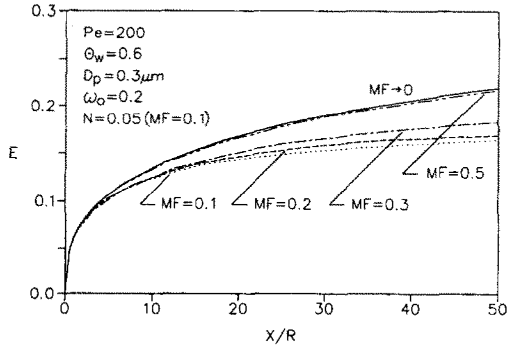

FIG. 11. Cumulative deposition efficiency for various particle mass fraction.

MF is always accompanied by the increase in thermal loading ratio C_L and absorption coefficient κ_0. Increase of thermal loading ratio decreases the mixture thermal diffusivity $(\alpha/(1+C_L))$ and then interrupts heat transfer. The increase of absorption coefficient κ_0 increases optical thickness τ_0, and conduction–radiation parameter N which contains an extinction coefficient. Thus we introduce the reference value of N when $MF = 0.1$. Figures 9–11 are the cases where the reference value of N is 0.05. As MF increases from 0.1 to 0.7, N increases from 0.05 to 1.0511 with constant inlet temperature T_{in}. These variations of N and τ_0 according to MF are listed in Table 1. The thermophoretic transport characteristics for MF less than 0.1 have been treated in the preceding work [14]. In high temperature applications, the interaction of radiant energy with the particulate phase can profoundly increase the heat transfer due to the large absorptivity of fine particles unless the particle mass fraction becomes high (i.e. the range from '$MF \to 0$' to '$MF = 0.1$' in Fig. 9). However, in the case of high particle mass fraction, excessive increase of absorption coefficient reduces the mean free path (mean penetration length) of a photon and, as a result, it interrupts energy transport from hot core region to cold near wall region. Therefore, Fig. 9 shows the development of mixed-mean temperature decreases as particle mass fraction increases from 0.1 to 0.5. The thermophoretic velocity increases as MF increases except for the central core of entrance region ($r/R < 0.4$, $x/R = 10$). In the central core of entrance region, when $MF = 0.5$, the thermophoretic velocity is lower than that of $MF = 0.2$ and 0.3, but exceeds those easily as fluid flows downstream (Fig. 10). Cumulative deposition efficiency increases with MF (Fig. 11).

In order to see the particle mass loading effect clearly, the overall view of the total deposition efficiency E_T is represented in terms of N and MF in Fig. 12. Brownian coagulation may be important when the particle mass fraction is more than 0.5 in this study. However, it is neglected because we mainly study the effect of particle mass fraction on the thermophoretic deposition. In the case of neglecting radiation, E_T increases with the increase of MF. This behavior is explained as follows. MF increases the thermal loading ratio C_L. And then, it causes a slower thermal development and flat and high temperature profile in the central core region. Therefore, near the wall, the temperature gradient becomes large and thermophoretic velocity increases. However, outside the near wall region, the temperature gradient becomes small due to the flat and high temperature profile and then the thermophoretic velocity decreases. Thus the total deposition efficiency, E_T, has a weaker MF dependence. The increase of the specific heat ratio ($C_H = C_{pp}/C_{pg}$) also makes the thermal loading ratio increase. Thus, the total deposition efficiency E_T increases as the specific heat ratio C_H increases. In the presence of radiation, the conduction–radiation parameter N, which contains extinction coefficient, has the reference values when $MF = 0.1$ (Table 1). The conduction–radiation parameter N represented in Fig. 12 are the values when $MF = 0.1$, and the variation of N and τ_0 according to MF are listed in Table 1. The decrease of the reference value N at $MF = 0.1$ (from 0.5 to 0.005 in Table 1) represents the increase of inlet temperature T_{in}. As the reference value of N becomes small, radiative heat transfer becomes predominant and the mixture temperature is more rapidly developed. Therefore the total deposition efficiency E_T becomes smaller with the decrease of reference value N under constant MF, similar to the N dependence in Fig. 5. When MF is less than 0.1, cumulative deposition efficiency also decreases as N decreases or $\tau_0(MF)$ increases [14]. However, when MF is more than 0.1, E_T has the minimum value at a certain MF according to τ_0 and N. In the case of $N = 0.01$ in which radiative heat transfer is predominated, E_T has the minimum value at $MF = 0.2$. The particle mass fraction which has a minimum value of E_T increases as the reference value N decreases.

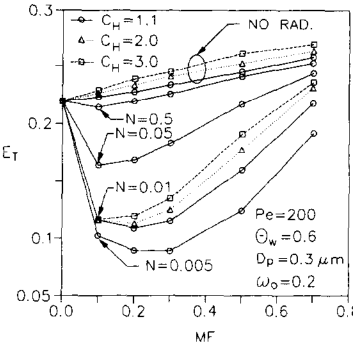

FIG. 12. Overall view of the total deposition efficiency with variation of conduction–radiation parameter, particle mass fraction and specific heat ratio.

Table 1. Variations of conduction–radiation parameter and optical thickness according to particle mass fraction

MF	N				τ_0
0.1	0.5†	0.05†	0.01†	0.005†	1.612
0.2	1.1261	0.1126	0.0225	0.0113	3.6271
0.3	1.9305	0.1931	0.0386	0.0193	6.2179
0.5	4.5045	0.4505	0.0901	0.0451	14.508
0.7	10.511	1.0511	0.2102	0.1051	33.853

† Reference value of N at $MF = 0.1$, and $\varepsilon_p = 0.9$.

4. CONCLUSIONS

The thermophoretic deposition of particles in the laminar tube flow has been investigated using the particle trajectory model and P-1 approximation. The effects of various conduction–radiation parameters, scattering albedo and particle mass fraction have been discussed on the thermophoretic particle transport characteristics. Based on the results, the following principal conclusions have been made.

(1) The thermophoretic deposition with the effects of radiative heat transfer and particle mass fraction is very important. As the radiative heat transfer effect becomes stronger, the fully developed thermal field is formed rapidly. Thus, thermophoretic deposition decreases.

(2) Radiative scattering due to particles tends to increase the thermophoretic deposition even if absorption remains constant.

(3) With the variation of particle mass fraction, there exists a minimum value of total deposition efficiency E_T depending on the optical thickness and the conduction–radiation parameter. The particle mass fraction which has a minimum value of total deposition efficiency increases as a reference value of the conduction–radiation parameter decreases.

Acknowledgement—We are grateful to Drs Y. J. Kim at KIMM and S. J. Yoa at National Fisheries Univ. of Pusan for helpful discussions and suggestions.

REFERENCES

1. D. E. Rosner and H. M. Park, Thermophoretically augmented mass, momentum and energy transfer rates in high particle mass loaded laminar forced convection systems, *Chem. Engng Sci.* **43**, 2689–2704 (1988).
2. S. L. Goren, Thermophoresis of aerosol particles in the laminar boundary layer on a flat plate, *J. Colloid Interface Sci.* **61**, 77–85 (1977).
3. M. Epstein, G. M. Hauser and R. E. Henry, Thermophoretic deposition of particles in natural convection flow from a vertical plate, *Trans. ASME, J. Heat Transfer* **107**, 272–276 (1985).
4. V. K. Garg and S. Jayaraj, Thermophoresis of aerosol particles in laminar flow over inclined plates, *Int. J. Heat Mass Transfer* **31**, 875–889 (1988).
5. K. L. Walker, G. M. Homsy and F. T. Geying, Thermophoretic deposition of small particles in laminar tube flow, *J. Colloid Interface Sci.* **69**, 138–147 (1979).
6. S. E. Pratsinis and K. S. Kim, Particle coagulation, diffusion and thermophoresis in laminar tube flows, *J. Aerosol Sci.* **20**, 101–111 (1989).
7. G. Vermes, Thermophoresis-enhanced deposition rates in combustion turbine blade passages, *Trans. ASME, J. Engng Power* **101**, 542–548 (1979).
8. D. E. Rosner and S. S. Kim, Optical experiments on the thermophoretically augmented submicron particle deposition from dusty high temperature gas flows, *Chem. Engng J.* **29**, 147–157 (1984).
9. A. D. Eisner and D. E. Rosner, Experimental studies of soot particle thermophoresis in nonisothermal combustion gases using thermocouple response techniques, *Combust. Flame* **61**, 153–166 (1985).
10. Y. J. Kim and S. S. Kim, Particle size effects on the particle deposition from non-isothermal stagnation point flows, *J. Aerosol Sci.* **22**, 201–214 (1991).
11. Y. J. Kim and S. S. Kim, Experimental study of particle deposition onto a circular cylinder in high-temperature particle-laden flows, *Experimental Thermal and Fluid Sci.* **5**, 116–123 (1992).
12. H. M. Park and D. E. Rosner, Combined inertial and thermophoretic effects on particle deposition rates in highly loaded dusty-gas system, *Chem. Engng Sci.* **44**, 2233–2244 (1989).
13. T. F. Morse, C. Y. Wang and J. W. Cipolla, Laser-induced thermophoresis and particulate deposition efficiency, *Trans. ASME, J. Heat Transfer* **107**, 155–160 (1985).
14. S. J. Yoa, S. S. Kim and J. S. Lee, Thermophoresis of highly absorbing, emitting particles in laminar tube flow, *Int. J. Heat Fluid Flow* **11**, 98–104 (1990).
15. C. T. Crowe, Review—Numerical models for dilute gas–particle flows, *Trans. ASME, J. Fluids Engng* **104**, 297–303 (1982).
16. L. Talbot, R. K. Cheng, R. W. Schefer and D. R. Willis, Thermophoresis of particles in a heated boundary layers, *J. Fluid Mech.* **101**, 737–758 (1980).
17. W. M. Kay and H. C. Perkins, *Handbook of Heat Transfer* (Edited by N. M. Rosenow and J. P. Hartnett), Chap. 7, pp. 1–54. McGraw-Hill, New York (1973).
18. S. K. Friedlander, *Smoke, Dust and Haze*, p. 32. Wiley, New York (1977).
19. F. H. Azad and M. F. Modest, Combined radiation and convection in absorbing, emitting and anisotropically scattering gas–particulate tube flow, *Int. J. Heat Mass Transfer* **24**, 1681–1698 (1981).
20. R. Echigo and S. Hasegawa, Radiative heat transfer by flowing multiphase medium—Part I. An analysis on heat transfer of laminar flow between parallel flat plates, *Int. J. Heat Mass Transfer* **15**, 2519–2534 (1972).
21. R. Echigo, S. Hasegawa and H. Tamehiro, Radiative heat transfer by flowing multiphase medium—Part II. An analysis on heat transfer of laminar flow in an entrance region of circular tube, *Int. J. Heat Mass Transfer* **15**, 2595–2610 (1972).
22. H. Tamehiro, R. Echigo and S. Hasegawa, Radiative heat transfer by flowing multiphase medium—Part III. An analysis on heat transfer of turbulent flow in a circular tube, *Int. J. Heat Mass Transfer* **16**, 1199–1213 (1973).
23. M. P. Mengüc and R. Viskanta, Radiative transfer in axisymmetric, finite cylindrical enclosures, *Trans. ASME, J. Heat Transfer* **108**, 271–276 (1986).
24. J. Higenyi and Y. Bayazitoglu, Differential approximation of radiative heat transfer in a gray medium, *Trans. ASME, J. Heat Transfer* **102**, 719–723 (1980).
25. C. T. Crowe, M. P. Sharma and D. E. Stock, The particle-source-in CELL(PSI-CELL) model for gas-droplet flows, *Trans. ASME, J. Fluids Engng* **99**, 325–332 (1977).
26. B. E. Pearce and A. F. Emery, Heat transfer by thermal radiation and laminar forced convection to an absorbing fluid in the entry region of a pipe, *Trans. ASME, J. Heat Transfer* **92c**, 221–230 (1970).
27. M. Kerker, *The Scattering of Light and Other Electromagnetic Radiation*, Chap. 4, pp. 118–127. Academic Press, New York (1969).